Specifying the equatorial ionosphere using CINDI on C/NOFS, COSMIC, and data interpolating empirical orthogonal functions

R. A. Stoneback,[1] N. K. Malakar,[1] D. J. Lary,[1] and R. A. Heelis[1]

Received 7 March 2013; revised 12 September 2013; accepted 23 September 2013.

[1] Data Interpolating Empirical Orthogonal Functions (DINEOFs) are a data-based method for determining a few orthogonal basis functions that optimally reproduce a given data set. This technique is applied to meridional drift measurements performed by the Coupled Ion Neutral Dynamics Investigation (CINDI) onboard the Communication/Navigation Outage Forecasting System (C/NOFS) as well as electron density profiles derived from GPS Radio Occulations (RO) performed by the Constellation Observing System for Meteorology, Ionosphere, and Climate (COSMIC). The low densities of the equatorial ionosphere spanning 2009–2010 restricted quality drift measurements by CINDI to altitudes near perigee, limiting the local time coverage of measurements. Full local time descriptions may be obtained as perigee moves through all local times though this requires a minimum 67 day season. To increase the data coverage of the ionosphere, CINDI data are supplemented with COSMIC GPS RO data. DINEOFs are applied to median meridional drift measurements as well as COSMIC measurements spanning 2009–2010 and are used to make a best estimate of the equatorial ionosphere at locations not observed. The scattered distribution of COSMIC profiles as well as the physical relationship between meridional ion drifts and the distribution of density with altitude improves the quality of the reconstructions compared to using CINDI alone. The DINEOF reconstructions demonstrate that the annual anomaly of reduced ionospheric densities in June compared to December measured by COSMIC is coincident with a change in the meridional ion drifts at the geomagnetic equator measured by CINDI.

Citation: Stoneback, R. A., N. K. Malakar, D. J. Lary, and R. A. Heelis (2013), Specifying the equatorial ionosphere using CINDI on C/NOFS, COSMIC, and data interpolating empirical orthogonal functions, *J. Geophys. Res. Space Physics*, *118*, doi:10.1002/jgra.50596.

1. Introduction

[2] Data Interpolating Empirical Orthogonal Functions (DINEOFs) [*Beckers and Rixen*, 2003] are a data-based method useful for reconstructing missing data in a data set using an empirical orthogonal function (EOF) basis. An iterative EOF decomposition of a sparse data set is performed to determine a limited set of orthogonal basis functions that optimally reconstruct the data set. For a given data slice from the set, missing values are determined by fitting the determined basis functions to known data. The fitted amplitudes may then be used along with the basis functions to fill in any gaps in the data slice. No a priori information about the data set needs to be specified. The technique has typically been applied to satellite data that contain measurement gaps due to the many challenges in forming a complete satellite data set.

[3] EOFs have seen widespread use in atmospheric science over several decades (see review by *Hannachi et al.* [2007]). Similar techniques have been used for the ionosphere; *Sun et al.* [1998] used the method of natural orthogonal components to isolate components of ionospheric currents driven directly by substorm processes using a chain of magnetometers. *Golovkov et al.* [2007] used the same method to generate a data-based model of the geomagnetic field in space and time. The model generated a main field that differed from traditional models by less than 10–15 nT. *Kim et al.* [2012] used a principal component analysis of Super Dual Auroral Radar Network data to perform a modal analysis of polar convection and determine the influence of the interplanetary magnetic field upon these modes. *A et al.* [2012] used global total electron content (TEC) data over 1999–2009 and were able to reconstruct 99% of the input variance using only four modes.

[4] DINEOFs have been applied to sea surface temperatures recorded by the Advanced Very High Resolution Radiometer satellite [*Beckers and Rixen*, 2003] with measurement gaps due to cloud coverage. A more complete treatment follows that also includes a comparison with optimal interpolation methods [*Alvera-Azcárate et al.*, 2005]. Errors on the order of 1°C are found for sea surface

[1]W. B. Hanson Center for Space Sciences, Physics Department, University of Texas at Dallas, Richardson, Texas, USA.

Corresponding author: R. A. Stoneback, W. B. Hanson Center for Space Sciences, Physics Department, University of Texas at Dallas, 800 W. Campbell Rd. WT 15, Richardson, TX 75080, USA. (rstoneba@utdallas.edu)

2169-9380/13/10.1002/jgra.50596

temperatures ranging between 16°C and 24°C. The DINEOF method can also be used to generate an error estimate for each missing data location along with the reconstruction of missing data [*Beckers et al.*, 2006].

[5] The method is amenable to operating on several scalar quantities at once. Sea surface temperatures, chlorophyll, and wind field measurements were analyzed simultaneously by *Alvera-Azcárate et al.* [2007], enabling a more accurate reconstruction of missing data than when using sea surface temperatures alone. Gaps in each of the parameters are filled in by DINEOFs. The performance on long data sets may also be improved by applying a filter function on measurements separated in time [*Alvera-Azcárate et al.*, 2009], ensuring that extremely sparse slices of data do not unduly influence the inferred missing data.

[6] The DINEOF process is applied here to equatorial in situ meridional ion drift measurements made by the Coupled Ion Neutral Dynamics Investigation (CINDI) onboard the Communications/Navigation Outage Forecasting System (C/NOFS) satellite. C/NOFS was launched in April 2008 into an elliptical orbit with perigee and apogee near 450, 850 km, respectively, with a 13° inclination. CINDI measures thermal plasma parameters as well as the ion drift in three dimensions [*Heelis and Hanson*, 1998]. Low ionospheric densities during the CINDI mission [*Heelis et al.*, 2009; *Stoneback et al.*, 2011] restricted quality drift measurements to altitudes near perigee, limiting the daily local time coverage of ion drifts. The DINEOF process is applied to the equatorial measurements of ion drift to fill in gaps in data coverage and produce a more complete map of equatorial ionosphere behavior.

[7] The impact of the low-data coverage upon the DINEOF reconstruction may be exacerbated by the distribution of the CINDI data. Perigee takes 67 days to move through all local times; thus, high-quality measurements at midnight are separated from high-quality measurements at noon by 33 days. This time span between measurements and the fact that drifts separated by 12 h of local time at a fixed longitude are infrequently simultaneously observed (due to altitude restrictions) do not provide a strong constraint on the basis functions in local time.

[8] To improve the DINEOF reconstruction, electron density profiles obtained from COSMIC GPS Radio Occultations (RO) are incorporated into the DINEOF process. COSMIC (Formosat-3) [*Cheng et al.*, 2006; *Lin et al.*, 2007b; *Lei et al.*, 2007a] is a constellation of six microsatellites launched in April 2006, each carrying a GPS RO receiver [*Schreiner et al.*, 2012]. Though in situ measurements from CINDI move slowly through local time, altitude profiles obtained from RO are scattered in local time. When C/NOFS perigee is located at midnight, daytime measurements of ion drift are unavailable. During this same time period, COSMIC will make measurements of the daytime ionosphere providing DINEOFs with more constraints on the state of the ionosphere. For ease of computation, the peak in ionospheric density, the altitude of the peak density, and a thickness parameter for the ionosphere are used to characterize the profiles rather than using the entire profile. These parameters are analyzed along with the CINDI data to produce a map of the equatorial ionosphere spanning 2009–2010.

[9] Here an overview of DINEOFs is provided, and the application to CINDI and COSMIC measurements is discussed. Results from the method and possible improvements in the application of DINEOFs to the equatorial ionosphere are also considered.

2. DINEOFs

[10] Consider a matrix $\mathbf{X}$ of size $m \times n$ containing measurements at m different locations in the equatorial ionosphere over n different times. The empirical orthogonal functions (EOFs) that best represent data $\mathbf{X}_{ij}$ for $i = 1 \cdots m$ and $j = 1 \cdots n$ may be obtained by using the Singular Value Decomposition (SVD) to rewrite this matrix as

$$\mathbf{X} = \mathbf{U}\Sigma\mathbf{V}^T \tag{1}$$

where $\mathbf{U}$ is a set of orthogonal spatial basis functions, $\mathbf{V}$ is the amplitude of the basis functions in time, and Σ is the matrix of singular values. It can be shown that the orthogonal basis functions $\mathbf{U}$ and $\mathbf{V}$ are the best representations of the data set $\mathbf{X}$ for a given number of modes [*Preisendorfer*, 1988; *Beckers and Rixen*, 2003]. When the SVD description is truncated to the N most significant modes, it provides a data reconstruction $\mathbf{X}'$ that is smoother than the supplied data in $\mathbf{X}$.

[11] This process may only be applied if data set $\mathbf{X}$ is complete, a situation not often encountered with satellite data. To overcome this limitation, an iterative EOF analysis is performed [*Beckers and Rixen*, 2003]. An initial estimate of the value of the missing data is made by using the spatiotemporal mean of the data. This estimate is used for all missing points, and an EOF analysis of this updated data set is performed and used to create a reconstructed set, $\mathbf{X}'$. The updated estimates for the missing data produced by the EOF in $\mathbf{X}'$ are used to replace the initial estimate of the missing data in $\mathbf{X}$ and the EOF process is repeated, producing a new $\mathbf{X}'$. The process iterates until the basis functions on successive iterations converge, producing both a set of functions that optimally reproduce the data as well as an estimate of all missing data points [*Beckers and Rixen*, 2003; *Alvera-Azcárate et al.*, 2005].

[12] The number of basis functions that optimally reproduce $\mathbf{X}$ is determined by a cross-validation technique. A portion of data within $\mathbf{X}$ is set aside and treated as missing. The root-mean-square (RMS) difference between the DINEOF reconstruction and the measured data is tracked as the number of basis functions determined via DINEOFs is varied. The reconstruction with the lowest RMS is chosen. DINEOFs employ the Lanczos solver [*Toumazou and Cretaux*, 2001] which has the desirable property that only the first N modes are actually calculated, minimizing calculation times for large data sets [*Alvera-Azcárate et al.*, 2005].

[13] The basis functions determined by the SVD will optimally reconstruct the data contained in $\mathbf{X}$. As physical drivers are not necessarily orthogonal, the basis functions will not generally isolate single physical drivers per basis function. EOF decompositions also tend to share similar characteristics [*Hannachi et al.*, 2007]. The lowest mode generally has wave number 1 and spans the whole domain. The next mode tends to have wave number 2 and will also be orthogonal to the first mode regardless of the physics of the system under study.

[14] Some techniques have been developed to enhance the physical interpretation of EOFs and a widely used

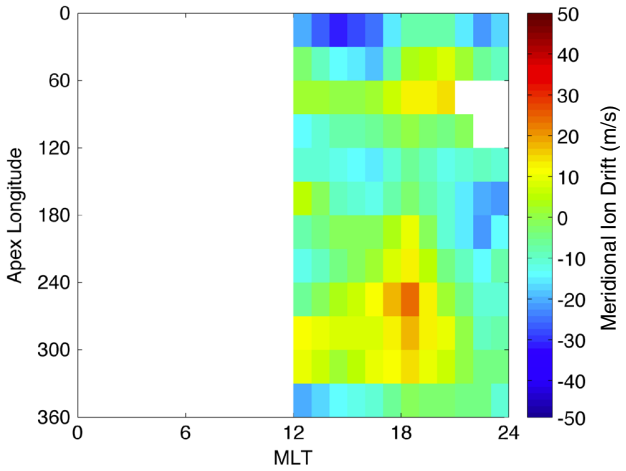

(a)

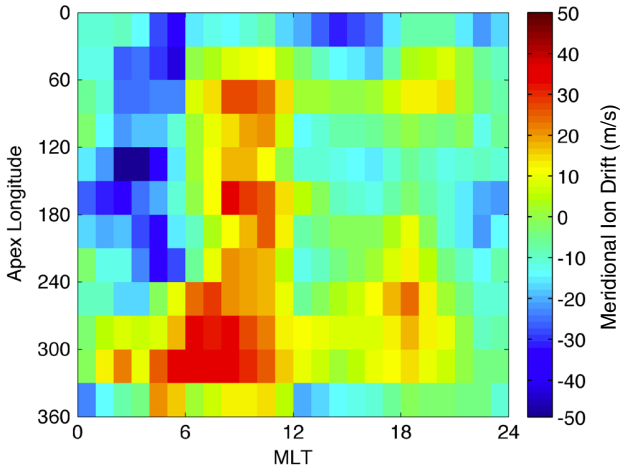

(b)

Figure 1. (a) Measurements of meridional ion drift from CINDI as a function of apex longitude and magnetic local time over all magnetic latitudes. The median drift for each bin is reported using measurements over 5 days, spanning DOY 256–260, 2010. (b) DINEOF reconstruction of meridional ion drifts over all longitudes and local times.

technique is known as rotation [*Hannachi et al.*, 2007]. If a constraint upon the system is available, the constraint could be applied to the basis functions to determine a combination of these functions that more closely satisfy the physical constraint. The general effectiveness of the method is limited by the need for an objective constraint upon the system. Despite the complications of interpreting the EOF basis modes for physical behaviors, the DINEOF results presented by *Alvera-Azcárate et al.* [2005] have identifiable physical sources in the basis functions. Thus, DINEOFs may be useful in increasing the physical understanding of the system at hand.

[15] The basis function determination involves a calculation of a covariance array, determining how each measurement location relates to every other measurement location. Thus, the arrangement of the spatial locations in **X** is not important. Multidimensional measurements of a system in

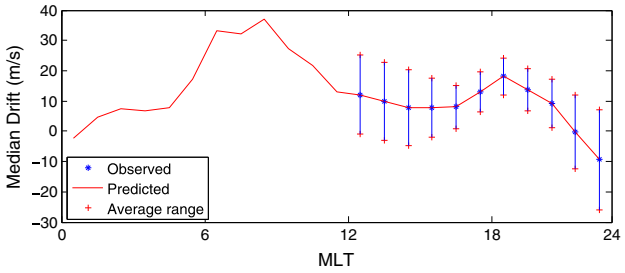

Figure 2. Measured and DINEOF reconstructed drifts in the 285° apex longitude sector (western pacific) for the same time period as in Figure 1.

time are treated simply as a one-dimensional array in space with measurements in time. This generality allows for any spatial distribution of measurements and may also be used to combine measurements of different physical parameters [*Alvera-Azcárate et al.*, 2007]. COSMIC and CINDI data may be analyzed together simply by putting both data sets into separate rows in **X**. Due to the different physical units of each measurement parameter (ion drift, peak density, etc.), for each parameter, the spatiotemporal mean over the respective data set is subtracted and then the data is normalized to have an absolute maximum value of 1.

[16] In addition, parameters that do not have a specific spatial location but are expected to have a common variation with other parameters in the data set may also be incorporated. For equatorial ionosphere studies, the state of the Sun and the magnetosphere can have a significant impact upon the state of the ionosphere. The strength of ultraviolet (UV) emissions from the Sun is commonly characterized by using the strength of 10.7 cm radio emission as a proxy as it is easily measured from the ground. The impact of UV upon the ionosphere varies as a function of local time, location, season as well the state of the Sun in its 11 year solar cycle. The covariance matrices determined in the DINEOF process allows a $F10.7$ index to influence the reconstruction of the whole data set where appropriate without having to specify the relation between $F10.7$ and the ionosphere. Similarly, solar wind parameters, interplanetary magnetic field strength and orientation, and *Kp*, *Ap*, or *Dst* indices may be used.

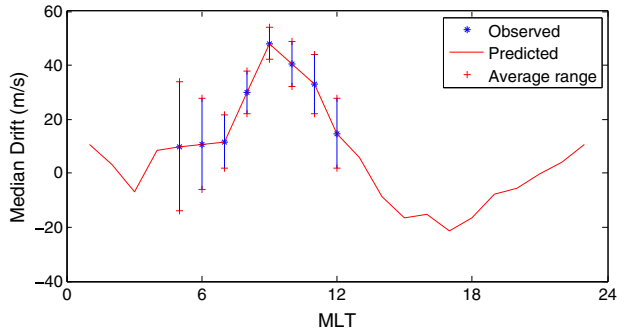

Figure 3. Measurements of meridional ion drift (blue) spanning 270°–300° apex longitude (western Pacific) along with average absolute deviations from the median spanning 36–40, 2010. The DINEOF reconstruction of drifts at all local times is in red.

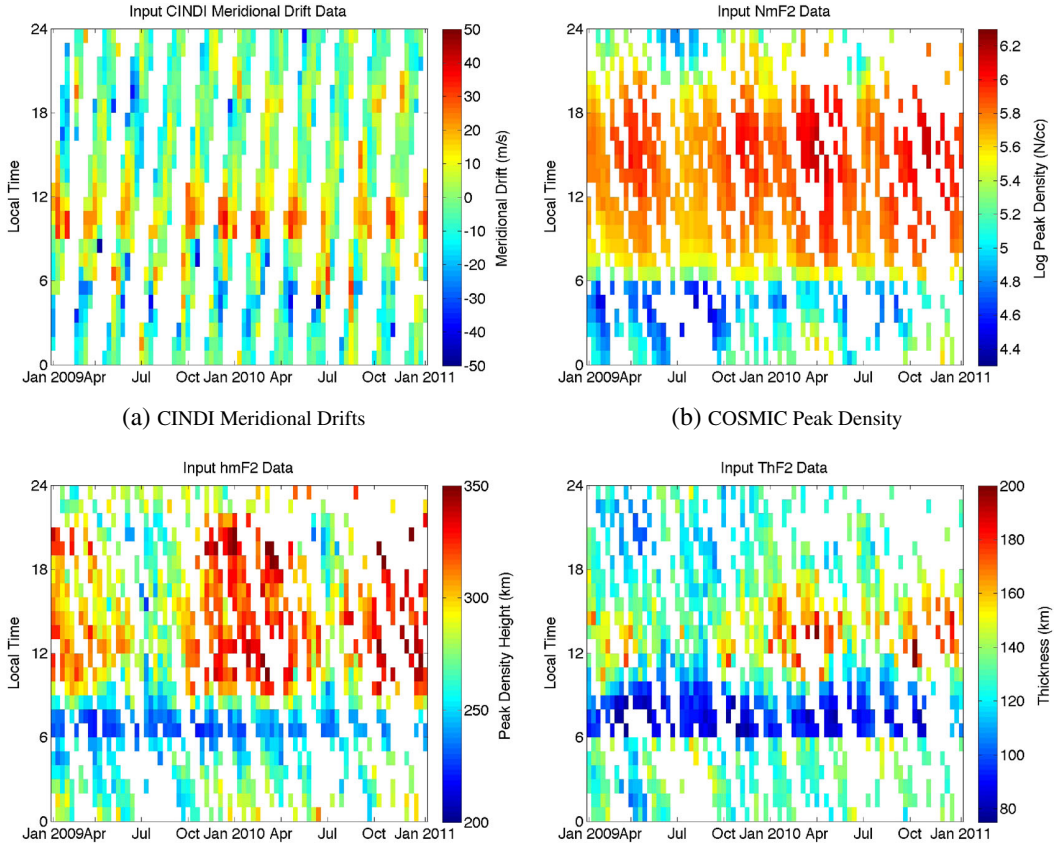

(a) CINDI Meridional Drifts (b) COSMIC Peak Density

(c) COSMIC peak density height (d) COSMIC thickness

Figure 4. CINDI and COSMIC data using 9 day medians and 1 h local time bins.

These parameters may also be included as new rows in **X**, where each measurement type is modified to have a mean of zero and an absolute maximum value of 1.

3. Results

[17] To apply the methods above to a description of equatorial ionosphere dynamics, the median of in situ measurements of meridional drift from CINDI over 5 day increments was calculated and binned by magnetic local time to produce the data set **X** for DINEOF analysis. Note that the number of data days per median does not remain constant throughout this work. The data are restricted to altitudes below 550 km subject to an O+ density minimum of 3×10^3 N/cc and 100 samples per bin are required. A 5 day period was used to smooth some of day-to-day variability in the ionosphere and increase data coverage. Though the DINEOF process can in principle handle data on a daily basis, there was insufficient data for 2009/2010 to sufficiently constrain the DINEOF process and produce reasonable predictions for missing data.

[18] Median drifts measured by CINDI were averaged with 2 h bins in magnetic local time (MLT), 30° apex longitude sectors, and drifts over all magnetic latitudes were allowed. The medians over 2 h time bins were interpolated to 1 h bins. With these restrictions, there is less than 50% data coverage from CINDI measurements. Missing data values for 2009 and 2010 were filled in separately with DINEOFs. An example of the meridional drifts for day of year (DOY) 256–260, 2010, one of the data slices input to the method, is shown in Figure 1a. The basis functions determined by DINEOFs are used to fill in drifts in the remaining local times in Figure 1b. Peak upward drifts are found near 10 MLT between 0° and 180° apex longitude and are found a bit earlier in local time between 240° and 360°. Three peaks are seen in the upward meridional drifts near 90°, 180°, and 270°, displaying longitudinal variations with a character similar to tidal patterns in the ionosphere. *Huang et al.* [2012] report tidal signatures in meridional drift velocities for CINDI data spanning November 2008 through Fall 2009. A wave 4 pattern is seen most strongly in the February–April and August–October periods, with peaks near 90°, 180°, and 270° and across 360°, 0° geographic longitude. Apex and geographic longitudes differ by about –70° at the magnetic equator; thus, the peaks in Figure 1b are shifted relative to *Huang et al.* [2012]. With the exception of the peak across 90° geographic longitude (20° apex longitude) reported by *Huang et al.* [2012], similar peaks are reconstructed by DINEOFs.

[19] A slice from the Pacific sector (285°) in Figure 1b is shown in Figure 2. Weak afternoon drifts are observed with a peak upward drift after sunset followed by downward drifts. The remaining local time sectors are reconstructed using DINEOFs. Upward drifts after midnight are observed, increasing after dawn with a peak near

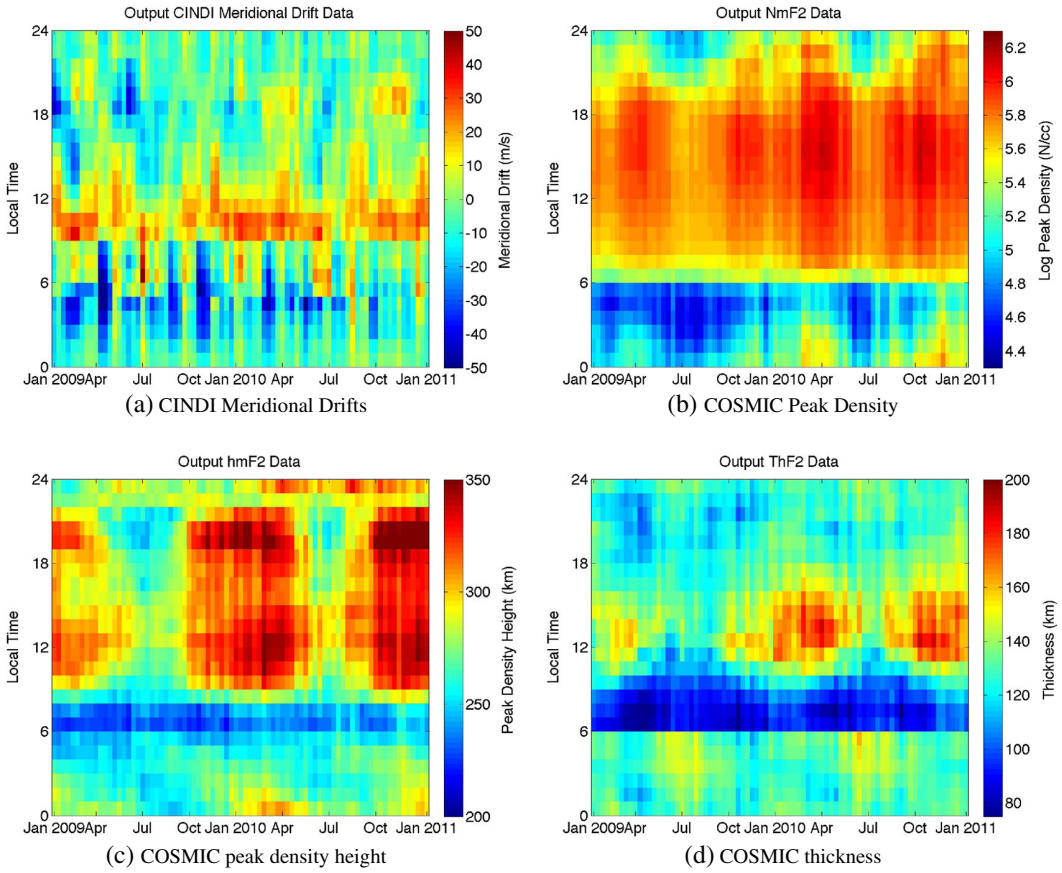

(a) CINDI Meridional Drifts (b) COSMIC Peak Density

(c) COSMIC peak density height (d) COSMIC thickness

Figure 5. DINEOF reconstruction using the 9 day median data shown in Figure 4.

10 MLT. The overall functional form of the ion drift is reasonable when compared to general expectations, though the particular value of the reconstructed drifts have not been validated.

[20] Some support for the DINEOF ion drift reconstruction may be found after a Sudden Stratospheric Warming (SSW). Previous measurements of drifts after an SSW event in 2008 reported by *Chau et al.* [2009] showed an increase in upward drifts in the morning along with downward drifts in the early afternoon. A major SSW occurred in late January 2010 with a westerly mean flow reversal between 24 and 26 of January and a peak in temperature at 60°N on 30 January [*Kuttippurath and Nikulin*, 2012]. A drift signature similar to *Chau et al.* [2009] is seen in the DINEOF reconstructed drifts from CINDI measurements in the Pacific longitude sector covering 5–9 February 2010, shown in Figure 3. Peak upward drifts above 40 m/s are observed, and the DINEOF reconstruction yields downward drifts in the afternoon of –20 m/s, similar to previous observations by *Chau et al.* [2009]. Though only one SSW event was observed in 2010 by DINEOFs, the meridional drifts observed at the equator are not the result of new physical modes. Rather, the change in the high-latitude wind field alters the magnitude of existing modes [*Fuller Rowell et al.*, 2010; *Goncharenko et al.*, 2010]. Though the DINEOF modes are not necessarily physical, the modes determined over a long data set may be expected to effectively describe short-term events such as a SSW.

[21] The expected error of the reconstruction is determined by withholding a portion of the data set and comparing the value filled in by DINEOFs and the measured value. The minimum RMS value obtained is in excess of 25 m/s. In general, DINEOF reconstructions, when there is daytime CINDI data, perform better than time periods without. Though the DINEOF reconstructions shown are consistent with established ionospheric behavior, the comparatively large RMS error indicates this is not always the case. The limited coverage of CINDI data and the distribution of the data is insufficient to properly constrain DINEOFs, i.e., perform viable reconstructions over apex longitude, local time, and time of year.

[22] In an effort to reduce the reconstruction error, the complexity of the problem is reduced; thus, median CINDI data over 9 day increments using 1 h bins in local time are used rather than the 5 day medians presented earlier and in addition all longitudes are averaged together. CINDI ion drift measurements are restricted to locations near the magnetic equator, ±5 magnetic latitude (MLAT). To further constrain the DINEOF process, COSMIC measurements of peak density (NmF2), the height of peak density (hmF2), and an ionospheric thickness parameter (ThF2) are also utilized. The thickness of the ionosphere is determined by calculating the effective-scale height above hmF2, the altitude range where densities are greater than NmF2/e. COSMIC data within 15° of the geographic equator were allowed and averaged using the same binning and time spans as CINDI.

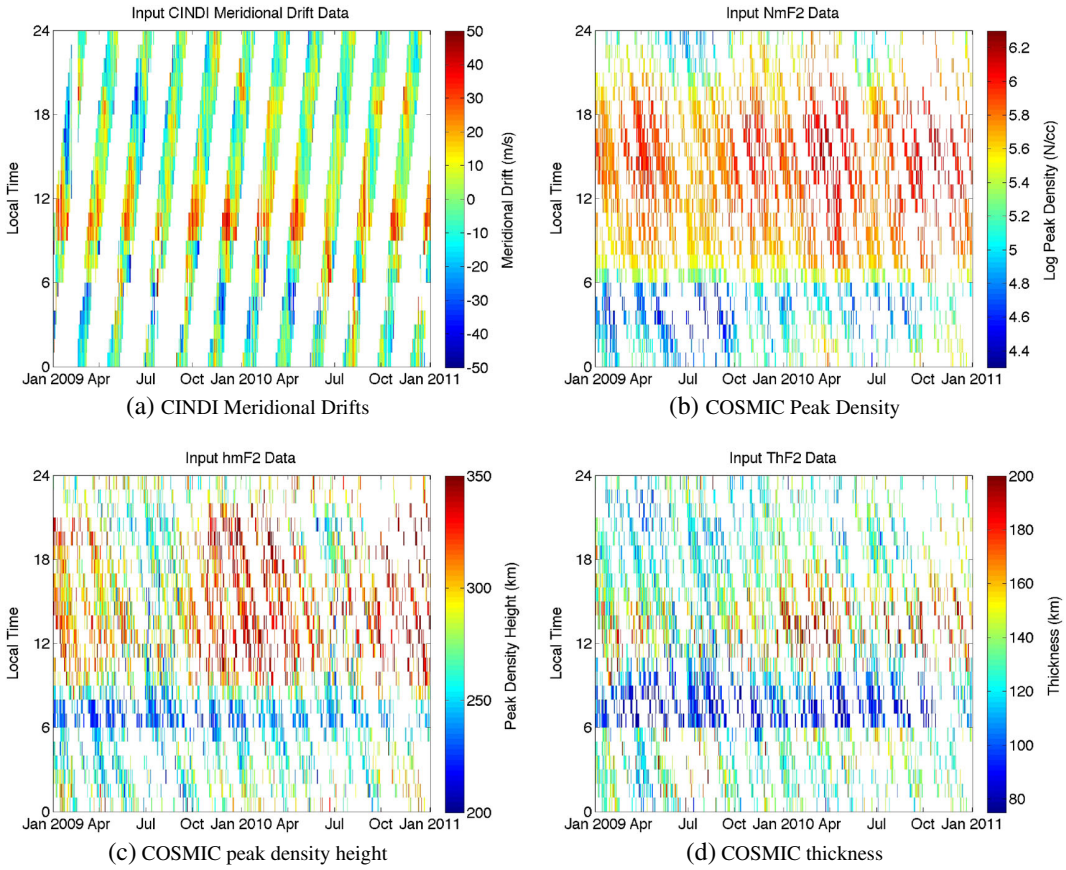

(a) CINDI Meridional Drifts (b) COSMIC Peak Density

(c) COSMIC peak density height (d) COSMIC thickness

Figure 6. Input data using 1 day medians.

A minimum of 5 COSMIC observations per local time is required. Generally, there are 5–10 ROs per local time bin per day for each reported median.

[23] The raw COSMIC GPS measurements are converted to electron density profiles by making a set of assumptions about the ionosphere and using the Abel transform. These assumptions break down when there are large horizontal gradients in the ionosphere. Errors are found within the E-region as well as at low latitudes. The derived parameters NmF2 and hmF2 are less affected by these errors and are generally reliable [*Yue et al.*, 2010]. Profiles are restricted to derived hmF2 altitudes between 175 and 475 km. The profiles provided by COSMIC Data Analysis and Archive Center (CDAAC) may also contain errors due to cycle slips or multipath signals [*Hwang et al.*, 2010]. These distorted profiles are excluded by filtering profiles with sharp density gradients.

[24] CINDI and COSMIC inputs are shown in Figure 4. The tracks of CINDI data are a result of measurements limited to local times near perigee and the 67 day movement of perigee through all local times. The COSMIC data are generally more complete than CINDI and have a more varied distribution. The satellite measurements in Figure 4 are supplied to DINEOFs along with 9 day means of $F10.7$ and *Dst*. To encourage the generation of seasonal modes by DINEOFs, a sine and a cosine wave are supplied with a yearly period and maxima at the equinox and solstice, respectively. Sinusoidal functions are chosen due to the periodicity of seasonal variations that are not effectively described with a linear day of year number. Both the sine and cosine are functions of day number and when used together uniquely index each day of the year while also linking the end of one calendar year with the beginning of the next. The same seasonal waveforms have been used when estimating TEC values using a neural network [*Habarulema et al.*, 2011]. Nine day means of these waveforms are also supplied to DINEOFs.

[25] The DINEOF reconstructions are shown in Figure 5. Peak upward meridional drifts are typically seen near 10 MLT in Figure 5a, though there are some deviations during the June solstices with peak upward drifts near dawn. Downward drifts are seen before sunset during the June solstices as well as in January of 2009 and 2010. Strong downward drifts are observed after midnight and through dawn in the period from January 2009 to July 2010.

[26] The DINEOF reconstructed peak density (NmF2) is shown in Figure 5b. The largest densities are observed during the equinoxes, with the lowest peak densities during the June solstices. The reduction in density is consistent with the reduced upward drifts through the day and downward drifts in the afternoon through sunset shown in Figure 5a. Reductions in NmF2 are also observed with the downward afternoon drifts in January of 2009 and 2010.

[27] The peak height (hmF2) is shown in Figure 5c. The largest peak heights are found during the December solstices, with minima in June. There is also a general increase from 2009 to 2010, consistent with increasing $F10.7$ levels.

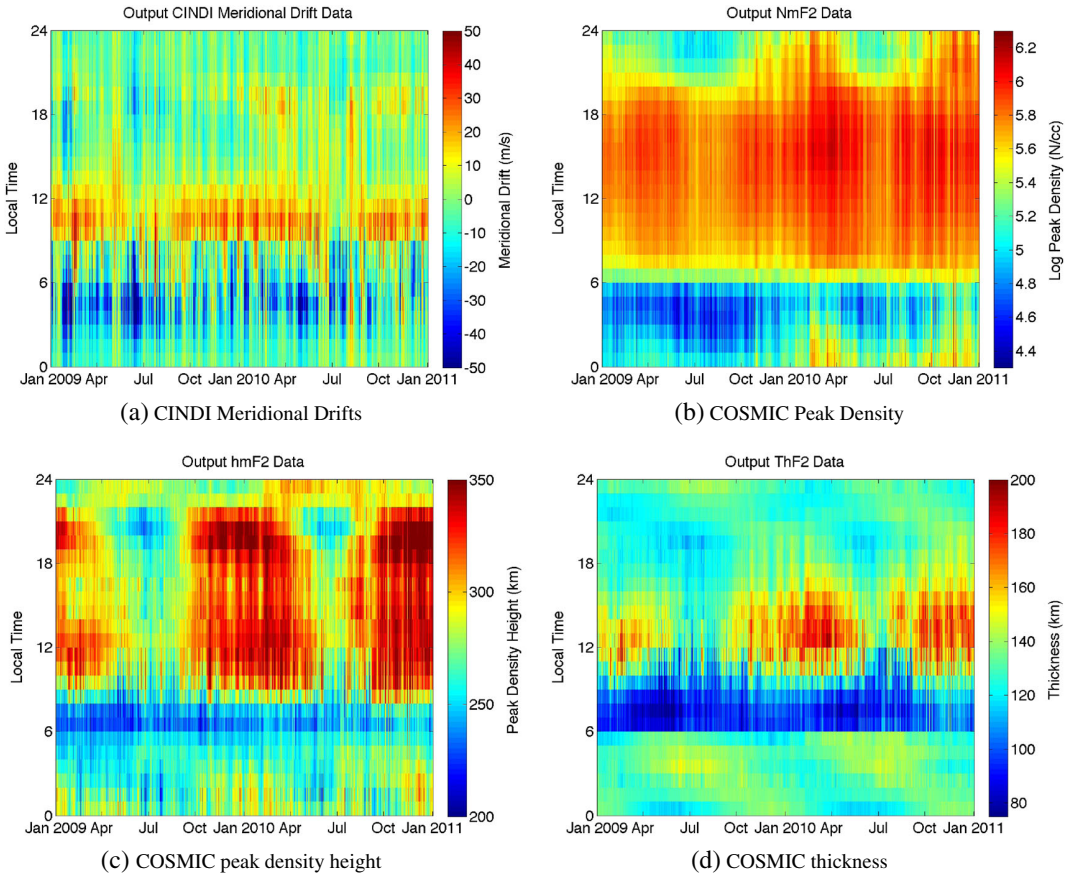

(a) CINDI Meridional Drifts (b) COSMIC Peak Density

(c) COSMIC peak density height (d) COSMIC thickness

Figure 7. DINEOF reconstruction of the ionosphere using 1 day medians of CINDI, COSMIC, and the relevant space weather parameters.

[28] The thickness above the density maximum (ThF2) is shown in Figure 5d. In local time, the smallest ThF2 is seen just after dawn and the commencement of photoproduction. The thickness generally increases through the day, influenced by the meridional ion drift. Upward/downward movement of ions during the day is expected to thicken/thin the ionosphere, as seen in the reconstructions. The maximum daytime thickness is found during the December solstice and equinox, coincident with the largest upward meridional drifts. At nighttime, the largest thickness is found during the June solstice. We will show that these increases in thickness are also coincident with an upward perturbation to ion drifts after midnight during the June solstice, not clearly visible in Figure 5a due to the color scale.

[29] Figures 6 and 7 contain the input data and DINEOF reconstructions when using median CINDI and related data on a 1 day basis using 1 h MLT bins. COSMIC has significantly less coverage than in the 9 day example. Despite the lower data filling factor, the general characteristics of the reconstruction match those in the 9 day medians in Figure 5. Though these global averages of ion drift, NmF2, hmF2, and ThF2 in longitude over equatorial latitudes can not be directly confirmed, the similarity of the 1 day reconstructions compared to the 9 day medians supports the DINEOF process on this shorter timescale.

[30] In general, seasonal changes of the ionosphere are reflected in all of the ionospheric parameters in Figures 5 and 7. This is to be expected from the DINEOF reconstruction. Each mode determined by DINEOFs spans meridional ion drift, NmF2, hmF2, ThF2, $F10.7$, *Dst*, as well as the seasonal sine and cosine inputs. Each mode has a single amplitude at each time for all parameters; thus, a change in a given modal amplitude to alter the reconstruction for a single parameter necessarily changes the reconstruction of the other quantities. The overall reconstruction provided by DINEOFs thus reflects a best fit of the ionosphere for all supplied measurement parameters. While the physical relationship between parameters has not been specified, the various parameters within a single mode are coupled through covariance in the data. Note, however, that the action of a physical source on the ionosphere could have a DINEOF description spread across multiple modes.

[31] The mode with the single largest contribution to the reconstruction is shown in Figure 8 with unit amplitude. The horizontal line in each plot is the mean value of the input data set when supplied to DINEOFs and should be treated as an effective zero line when scaling the modal amplitudes. The dominant mode for meridional ion drifts in Figure 8a has downward drifts after midnight, with a maximum downward drift before dawn. After, dawn drifts increase peaking near 10 MLT, only to decrease and become downward shortly after noon. A slight prereversal enhancement (PRE) is seen just after sunset. The downward afternoon drifts in this mode are consistent with the reported downward afternoon drifts

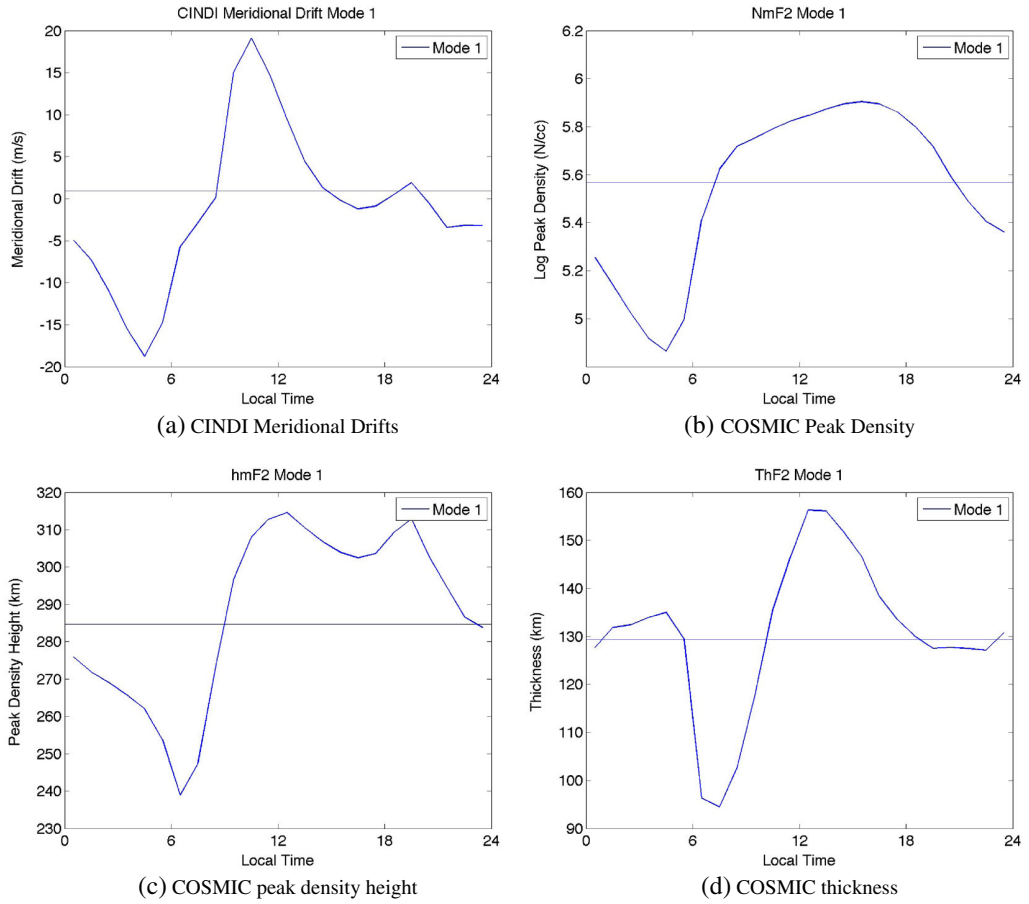

(a) CINDI Meridional Drifts (b) COSMIC Peak Density

(c) COSMIC peak density height (d) COSMIC thickness

Figure 8. Mode with the largest contribution to the DINEOF reconstruction shown in Figure 7 using 1 day medians.

obtained using seasonally averaged CINDI data over all magnetic latitudes observed by C/NOFS [*Stoneback et al.*, 2011], though the results here are restricted to locations near the magnetic equator.

[32] The peak density NmF2 is shown in Figure 8b; minimum densities are seen before dawn, rising quickly after dawn and throughout the day. Densities decrease after sunset and fall through the night, as expected for the ionosphere. The peak density height in Figure 8c is similar to the meridional drifts, increasing after dawn with a peak near noon. hmF2 falls after noon only to increase after sunset, consistent with the timing of the PRE in the ion drifts. Downward ion drifts are not necessarily inconsistent with the increase in hmF2 after sunset. The loss of photoproduction with sunset allows loss processes to exert more influence on the distribution of plasma in the ionosphere. Loss rates decrease with increasing altitude; thus, after sunset, the lower altitudes of the ionosphere are lost, raising the peak density height of the ionosphere, though NmF2 itself is lower.

[33] The ionospheric thickness in Figure 8d has a rise after sunrise and a decrease though the afternoon. As NmF2 and hmF2 fall through the night, the thickness of the ionosphere increases. Once photoproduction commences with sunrise, a thin ionosphere is found at the location of peak photoproduction.

[34] The amplitude of the DINEOF modes is shown in Figure 9 while the modes themselves are shown in Figure 10 with unit amplitude. Note that a given modal amplitude governs the contribution of that mode across all input measurement types. The modes are sorted in decreasing order of importance in reconstructing the variance of the input CINDI and COSMIC data set. Note that the variance contribution of each mode is a product of both the mode and its amplitude in time. The most dominant mode, highlighted in Figure 8, has a nearly constant amplitude over 2 years, interpreted as the average state of the ionosphere. The second mode is largest during the June and December solstices. During the June solstice, downward perturbations in meridional ion drift, NmF2, and hmF2 with an oscillation period of 8 h in local time are observed. The perturbation to hmF2 increases through the daytime hours, maximizing after sunset. The drift perturbation at this time acts against the PRE; thus, a downward perturbation in hmF2 is expected to counter the increase in hmF2 in the quasi constant first mode. The scale height above hmF2 is generally reduced through the day, with an increase after midnight and before dawn. The opposite contribution is generally found during the December solstices.

[35] The third mode has a clear sinusoidal variation with maxima near equinox. This mode leads to downward/upward drift perturbations after sunset through dawn

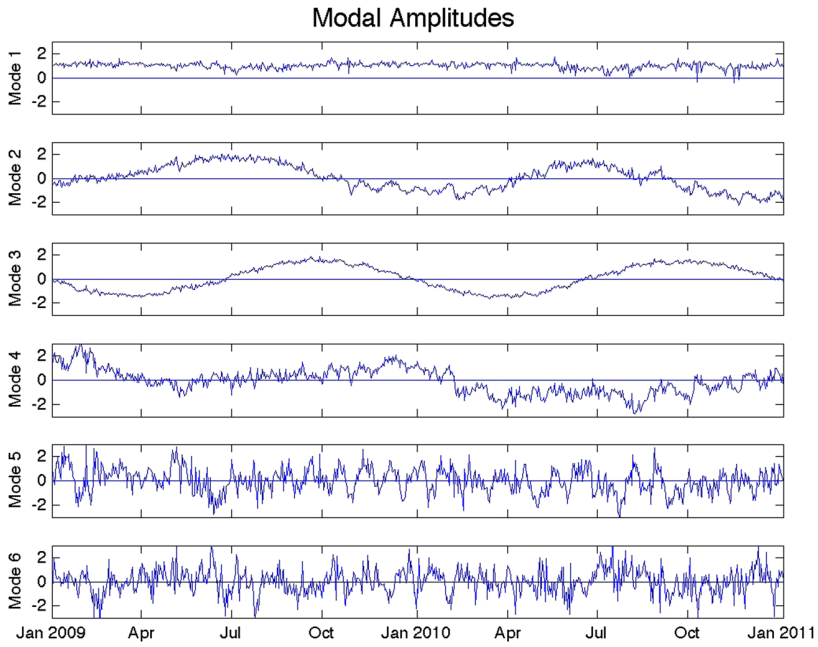

Figure 9. Amplitude of the DINEOF modes over 2009/2010 using 1 day median data.

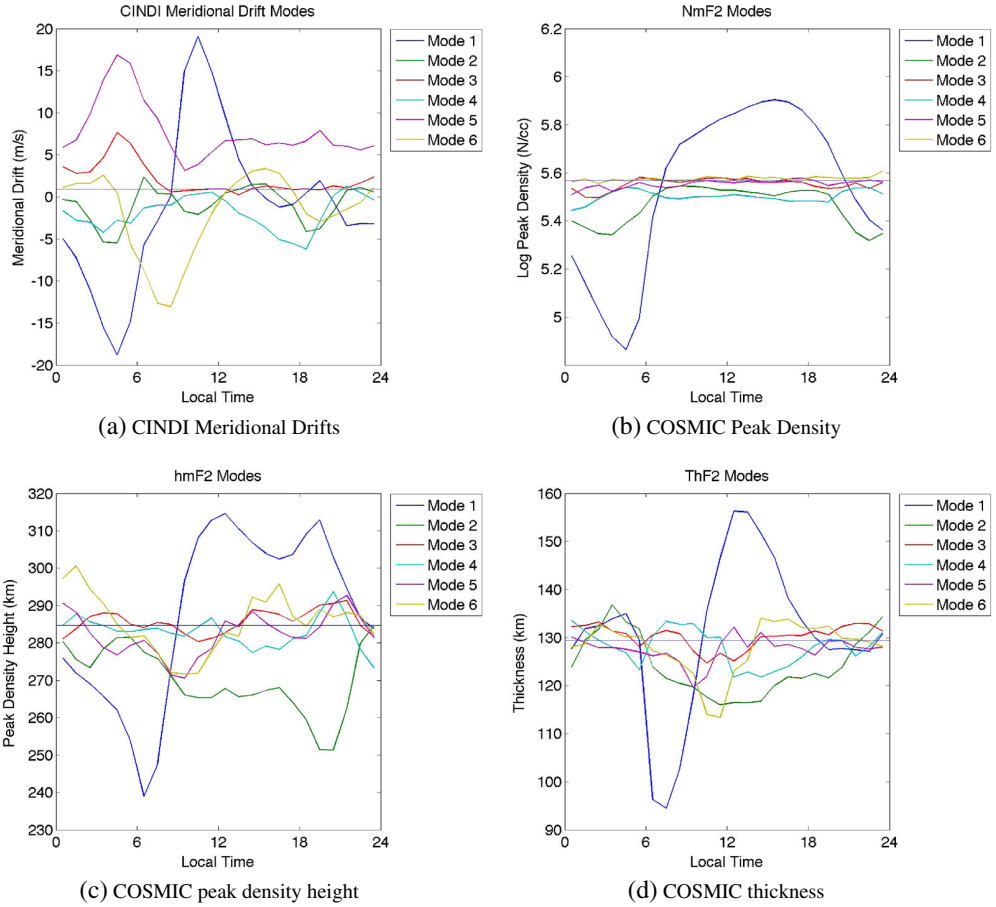

(a) CINDI Meridional Drifts

(b) COSMIC Peak Density

(c) COSMIC peak density height

(d) COSMIC thickness

Figure 10. DINEOF modes determined using data shown in Figure 6 and 1 day medians. While each DINEOF mode spans all input parameters, only the meridional drift, NmF2, hmF2, and ThF2 results are shown here. The space weather parameter portion of these modes is shown in Figure 11.

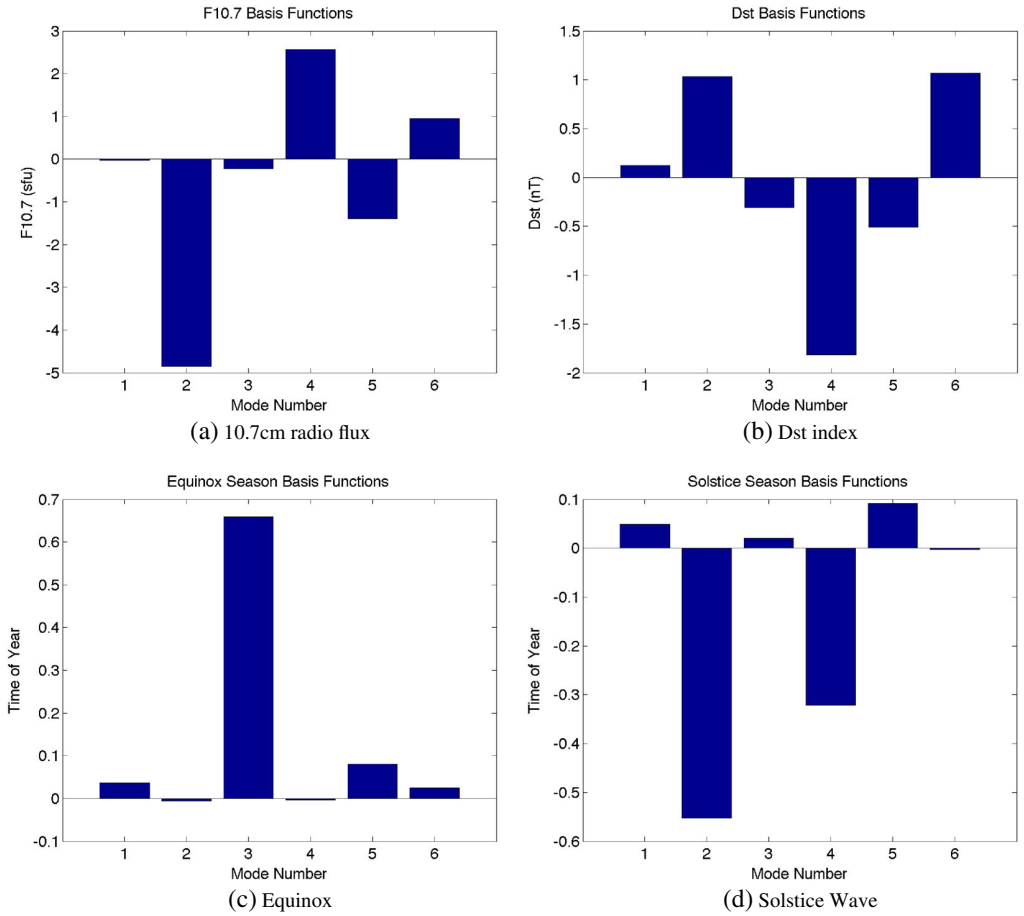

(a) 10.7cm radio flux (b) Dst index

(c) Equinox (d) Solstice Wave

Figure 11. DINEOF modes determined using data shown in Figure 6. The contribution of these modes to the space weather parameters is detailed. As each mode spans all input parameters, the corresponding variations in the remaining parameters (NmF2, hmF2, ThF2, meridional ion drift) for these modes are shown in Figure 10.

in the autumn/spring; however, this corresponds with an increase/decrease in NmF2 during the nighttime hours. NmF2 is primarily driven by solar inputs; thus, a complete correlation with meridional drifts is not expected. Variations in hmF2 and ThF2 have similar and consistent waveforms in local time.

[36] Modes 4–6 have variations accounting for shorter term variations in the ionosphere. Mode 5 has a clear periodic oscillation in Figure 9 with a period near 30 days from October 2009 to January 2010. Mode 5 also has a meridional drift variation with a nonzero average in local time. The amplitude of this mode in time is periodic; thus, the long-term drift contribution to the ionosphere remains near zero. Mode 6 has downward drifts after dawn and corresponding decreases in hmF2 and ThF2.

[37] The product of the modal amplitudes in Figure 9 with the DINEOF modes leads to reconstructions in all parameters. For ion drifts, NmF2, hmF2, and ThF2, the DINEOF modes describe variations over 24 h of local time. For the key indices, the modes are a single number rather than a waveform in local time. Bar charts detailing the modes for $F10.7$, *Dst*, and the seasonal sine and cosine inputs with unit amplitude are shown in Figure 11. The values plotted are deviations from the mean of each particular input. For $F10.7$, mode 2 has the largest component, with decreasing contributions from modes 4, 5, and 6. For *Dst*, mode 4 has the largest component. Modes 2 and 6 have similar magnitudes, half as large as mode 4.

[38] Mode 3 is significantly larger in Figure 11c than the other components and thus will have a dominant contribution to the equinox waveform when all modes have a similar amplitude. The amplitude of mode 3 in time in Figure 9 also follows a sinusoidal oscillation, demonstrating that it is the dominant mode in reconstructing the equinox waveform. For the solstice variation, mode 2 in Figure 11d is the largest, followed by mode 4. We can see that the amplitude of mode 2 is similar to a cosine; however, at the beginning of the data set where we would expect an absolute maximum, it is near 0. During this time, mode 4 has an amplitude near 2. So while mode 2 generally accounts for solstitial variations in the ionosphere, there can be significant contributions to this seasonal behavior from mode 4. Note that modes 2 and 4 also have nonnegligible contributions to the reconstruction of $F10.7$ and *Dst*. Thus, variations in the ionosphere with solstice are spread across more than one mode.

[39] In Figure 12, we can see that DINEOFs have been able to reproduce the variations in $F10.7$ cm flux and season fairly well. The input and reconstructed *Dst* are shown

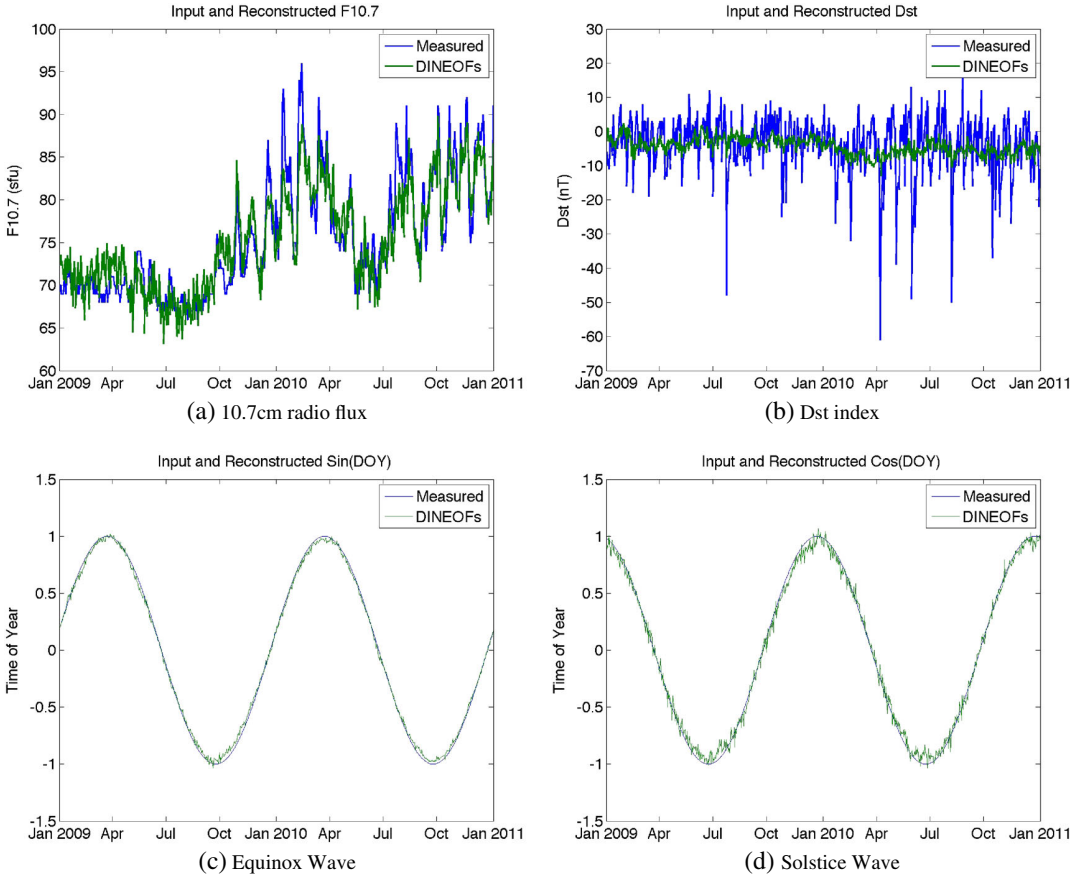

Figure 12. Input space weather parameters along with the DINEOF reconstructions of these inputs when accounting for all available data. DINEOF results generated using 1 day medians of CINDI and COSMIC.

in Figure 12b though the variations in the *Dst* index are not reproduced. Thus, the DINEOF modes have not been effective in associating changes in the ionosphere to changes in *Dst*, indicating that additional information is required. This is expected as the coupling between the mean *Dst* per day and the median equatorial ionosphere is low. Even if the full variation of *Dst* with universal time was included, the ionospheric measurements are the median value of all longitudes and universal times in each local time bin. Storm time effects are a strong function of universal time; thus, the median data here reduce any storm time signatures. This demonstrates that the DINEOF process can not arbitrarily reproduce all input data if there is insufficient covariance. While inputting the *Dst* index alone to DINEOFs will produce a viable reconstruction, the use of multiple measurements of the ionosphere constrains the DINEOF process.

[40] To get a better handle on the coupling of modes with the space weather parameters, the correlation between the time series of the modal amplitudes over 2009/2010 and the time series of the relevant parameter was calculated. Table 1 details the correlation for each mode and parameter, along with the percent of the variance in the input data signal that each mode accounts for. Though the dominant mode is quasiconstant, there are some low correlations with the solstice and equinox seasons. The correlation of the equinox waveform and mode 3 is very high (0.99), expected from the mode distribution in Figure 12c as well as the amplitude of the mode in time. This indicates that there is a systematic variation in the ionosphere with equinox. Mode 2 has significant correlations with both $F10.7$ and the solstice waveform. Mode 4 also has correlations with the same quantities though it is lower. This indicates that $F10.7$ and solstice variations have not been isolated to single modes.

[41] To demonstrate the influence of the additional COSMIC data to the DINEOF reconstruction, Figure 13 shows ion drift reconstructions when supplying DINEOFs with different data. In Figure 13a, the DINEOF process is only supplied with meridional ion drifts over 2009/2010 using 9 day medians. We use 9 day medians rather than daily values since the 9 day reconstructions are smoother, making large-scale variations easier to identify. There is a large variation

Table 1. Linear Correlation Between the Amplitude of Each Mode in Time With the Various Parameters[a]

Mode	$F10.7$	*Dst*	Equinox	Solstice	% Variance
1	0.04	0.06	0.21	0.30	50.8
2	0.74	0.18	0.02	0.85	20.1
3	0.05	0.03	0.99	0.02	7.9
4	0.44	0.25	0.03	0.53	4.6
5	0.23	0.04	0.11	0.15	4.5
6	0.15	0.13	0.03	0.01	3.7

[a]Data input to DINEOFs generated using 1 day medians.

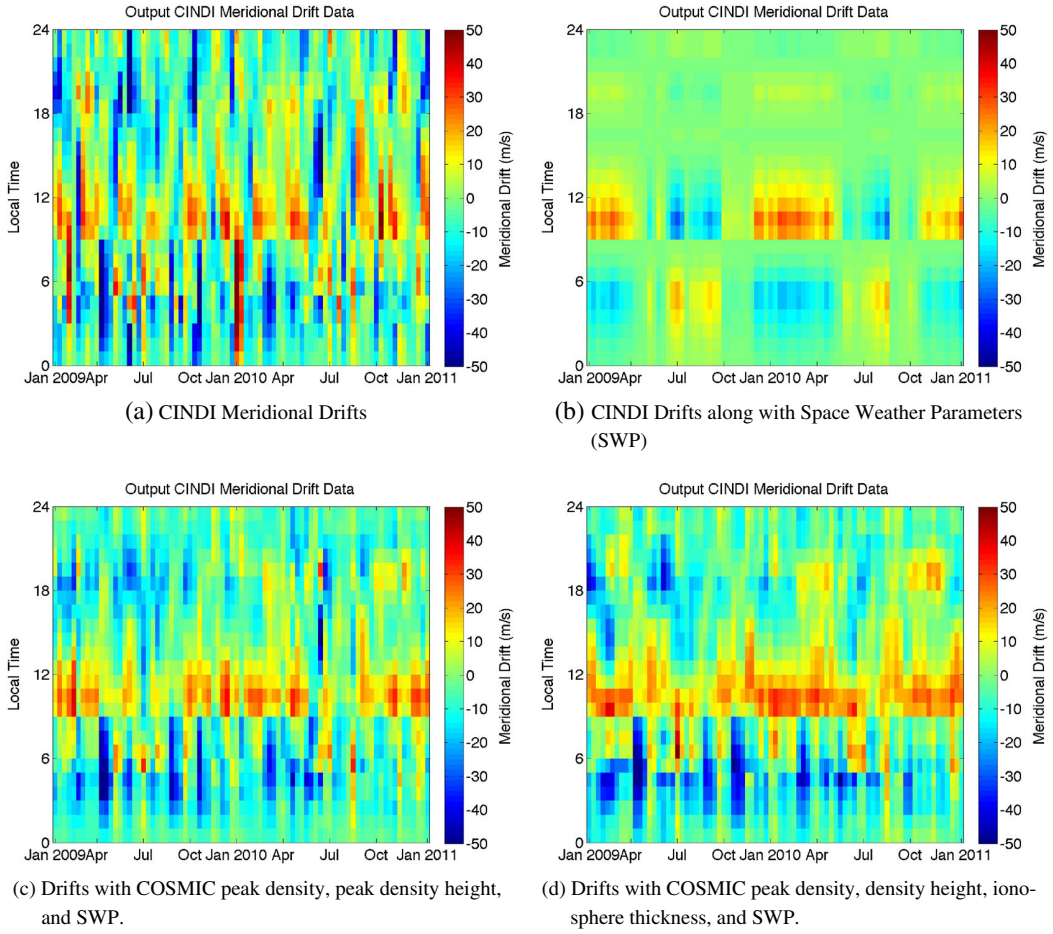

(a) CINDI Meridional Drifts

(b) CINDI Drifts along with Space Weather Parameters (SWP)

(c) Drifts with COSMIC peak density, peak density height, and SWP.

(d) Drifts with COSMIC peak density, density height, ionosphere thickness, and SWP.

Figure 13. DINEOF drift reconstructions with different input data sets.

in the drift reconstructions. Reconstructions near 10 MLT are generally upward when in situ measurements are made in the local time sector; however, as measurements drift to nighttime, the reconstructed drifts reduce in magnitude, even turning negative before noon. This periodicity in the data is a consequence of the local time distribution of CINDI data and not a reflection of the ionosphere itself. While the modes determined by DINEOFs will be orthogonal when considering all local times, over limited local times this is not required. Thus, the limited local time coverage provided by CINDI allows for multiple configurations of DINEOF modes that could adequately explain the provided measurements but result in significantly different reconstructions in areas not measured. To improve the reliability of the CINDI reconstruction, more information is required.

[42] In Figure 13b, the CINDI data are supplemented with basic space weather parameters, $F10.7$, Dst, and the seasonal sine and cosine functions. Only one mode is retained in this configuration, leading to a low resolution and smooth reconstruction of the ionosphere. While a single mode can not account for all the variations in the ionosphere, the seasonal changes shown are very consistent with the ionosphere thickness in Figure 10d. Upward drifts are seen near 10 MLT for the December solstice through the March equinox. From June to September, downward drifts are seen near 10 MLT with upward drifts from midnight through dawn. The variations outlined by this single mode agree well with the seasonal variation in the COSMIC observations even though COSMIC data have not been provided in this configuration.

[43] In Figure 13c, COSMIC NmF2 and hmF2 are also added. The downward drifts identified in Figure 13b are no longer as clear; however, a downward perturbation in daytime drifts is observed during the June solstice seasons. Overall, more of the variance of the input data is retained and daytime drifts in Figure 13a are a bit less influenced by the local time of CINDI perigee. While values of NmF2 and hmF2 are influenced by meridional drift, during the day the largest influence is from the Sun, limiting the constraint NmF2 and hmF2 fix on the meridional drift.

[44] In Figure 13d, COSMIC ThF2 is also included. This results in a smoother reconstruction and significantly removes the strong influence of CINDI perigee location on the reconstructions of ion drift. The thickness of the ionosphere is more strongly correlated with the meridional drift during the day which provides a more effective constraint upon the DINEOF reconstructions. The distributed local time coverage provided by COSMIC along with the physical relationship with the ion drifts that lead to common variations helps constrain the DINEOF predictions in areas not measured by CINDI, leading to a significantly more consistent reconstruction of upward drifts before noon over the data set. The downward perturbation to the meridional ion drifts in the daytime ionosphere identified in

Table 2. The Expected Error for Filling in Gaps in the Data Set as Well as the RMS Error Between the DINEOF Fitted Curves and the Input Data[a]

Data Set	1 Day	9 Day	1 Day	9 Day
Parameter	Expected Error		RMS Error	
Ion drift (m/s)	19.9	7.1	8.9	5.4
hmF2 (km)	26.1	13.4	16.9	9.2
Log NmF2 (cm^{-3})	0.28	0.16	0.10	0.05
ThF2 (km)	39.1	12.5	17.9	7.5
*F*10.7 (sfu)	4.6	2.1	2.7	1.9
Dst (nT)	12.7	3.1	7.9	4.5
Equinox	0.22	0.15	0.06	0.06
Solstice	0.22	0.15	0.03	0.03

[a]The expected error is generated by withholding 770 of the input data points from the process and comparing the reconstructed values to the measured values. The RMS error is determined by comparing all of the input data points to the DINEOF reconstructions.

Figure 13b is still visibly present, though drifts are generally still upward in the midmorning, consistent with expectations. The upward perturbation to drifts after midnight near the June solstices is also still present though the additional night time variability makes the signature less clear.

[45] Though a number of details present in input data are not reproduced by the final reconstruction, the loss of detail is outweighed by the improvement in general characteristics. The overall expected error on the normalized data set is 0.146, calculated by the DINEOF process using 770 data points treated as missing. Using the normalization constants for each measurement parameter, this leads to the expected errors listed in Table 2. The expected error characterizes DINEOFs ability to estimate values at unobserved locations using a sparse data set. The RMS error also listed in Table 2 characterizes DINEOFs ability to reproduce measured values in the ionosphere using the modes it has determined. It is determined by calculating the RMS error between all input data and the reconstructions. Predicting ion drifts in the ionosphere with DINEOFs has an expected error of 7.1 m/s. The target accuracy for cross-track in situ measurements of ion drift by CINDI is $\pm$5 m/s, limited by the pointing accuracy of the satellite [*Stoneback et al.*, 2012]. Though the reconstructions are not statistically as good as measurements, on average the error is only approximately 2 m/s larger than measurements. A DINEOF reconstruction in locations that have measurements has an RMS error of 5.4 m/s, close to the uncertainty in the CINDI measurements. This error characterizes both the limitations of the DINEOF modes as well as the deviation caused when making the reconstructions of one parameter consistent with all other measured parameters.

[46] For daily median, data filling in ion drifts has an error of 19.9 m/s; thus, the 1 day data are not currently capable of accounting for the full variability of the ionosphere in ion drifts. A portion of this error will account for biases in the input data, more prominent in the 1 day data than the longer 9 day averages. With a shorter averaging time frame, the results from both COSMIC and CINDI may not fully characterize each local time bin over all longitudes and equatorial latitudes. With only 5–10 ROs per local time bin per day, there will be variations in the longitudes and latitudes sampled by COSMIC. Despite these issues, the expected error for hmF2 is 26.1 km, less than 10% error for hmF2 outside of dawn.

4. Discussion

[47] The DINEOF process was able to successfully integrate measurements from both COSMIC and CINDI to produce a reconstruction of the ionosphere. The dominant modes identified in ion drift, NmF2, and hmF2 are consistent with known properties of the ionosphere [*Kelley*, 2009]. While ion drifts are generally positive in the afternoon at higher solar activity levels [*Fejer et al.*, 1991; *Kil et al.*, 2009; *Pacheco et al.*, 2010; *Fejer*, 2011], the waveform identified by DINEOFs is clearly consistent with the average ionosphere. Downward afternoon drifts during periods of low solar activity have been reported using CINDI data [*Stoneback et al.*, 2011], Vector Electric Field Instrument (VEFI) data [*Pfaff et al.*, 2010], as well as ground station measurements [*Patra et al.*, 2012] during the solar minimum period of 2009/10.

[48] The inclusion of the seasonal sine and cosine functions with the DINEOF process leads to a modal description that highlights seasonal variations. Changes to the ionosphere during equinox are captured very well by mode 3. As DINEOFs is purely data based, this demonstrates that there are systematic variations in the input data with season. While the fact that seasonal variations in the ionosphere occur is not new [*Burkard*, 1951; *Liu et al.*, 2009], it is still a topic of study [*Rishbeth*, 2004; *Fejer*, 2011]. The isolation of seasonal effects by providing a seasonal input suggests that other variations in the ionosphere due to a given input may be isolated by providing that input to the DINEOF process.

[49] However, simply including an index parameter is not always sufficient in isolating a response. Solstice variations are not isolated as cleanly due to correlations with the *F*10.7 index. Reductions in *F*10.7 tend to coincide with the June solstice seasons over the time period considered even though each process is completely independent. The variation in mean *F*10.7 is not very large over the time period investigated and only comprises a short fraction of a solar cycle. A longer data set with larger solar output variations would likely result in DINEOF modes that discriminate between *F*10.7 and seasonal variations more effectively. The long data set used by *A et al.* [2012] that spans 1999–2009 produced a base mode that is highly correlated with *F*10.7.

[50] Isolating ionospheric changes with the *Dst* index was not as successful as for the other parameters. The data used here averaged all longitude sectors together. Thus, for a given geomagnetic disturbance, measurements at a given local time will involve universal times both before and during the disturbance, weakening the underlying physical relationship between geomagnetic disturbances and ionospheric effects. Further, during the analysis period, variations in *Dst* are generally small and measurements are restricted to low latitudes. The stronger the physical connection between measurements is expressed in the data, the more effective the measurements will be in the DINEOF process. Thus, a strong storm time response with this configuration of inputs was not expected. There could be additional factors for the limited reconstruction of *Dst* such as time lags or even physical irrelevance. However, the median averaging of ionospheric data over all longitudes used here fundamentally smears any ionospheric response to magnetospheric

changes captured by *Dst* and thus is not well suited for *Dst* investigations. A more complete description of the ionosphere in longitude as well as the inclusion of additional data sets that characterize energy inputs at high latitudes may produce a more effective description of disturbance effects.

[51] Though the *Dst* effects were not isolated, this result demonstrates that the inclusion of multiple data sets limits the DINEOF process when determining the basis functions. While the DINEOF process is able to reconstruct the *Dst* index parameter without issue when provided alone, the constraints provided by multiple measurement types reduce the space of possible functions that could be used to reconstruct the data set. In situations where there is a lack of a systematic response in a large and varied data set to a given parameter, the DINEOF process is not expected to effectively describe those variations. Since a complete reconstruction of all inputs is not guaranteed in a varied data set, the successful isolation of a response to a given input parameter in the DINEOF process suggests that the mode derived is not arbitrary.

[52] COSMIC data used here were restricted to $\pm 15°$ geographic latitude (GLAT). Since the geographic latitude of the geomagnetic equator varies as a function of longitude, this introduces some variance in the COSMIC sampling. Increasing the latitudinal width of allowed measurements to $\pm 20°$ does not change any of the conclusions generated from the more restricted set. As expected, however, the increased data coverage does reduce the errors of the DINEOF process. Using geopack-2008, the magnetic latitude of the COSMIC measurements was generated and the DINEOF process was applied to data sets spanning $\pm 15°$ and $\pm 25°$ magnetic latitude (MLAT). The DINEOF results for these inputs are qualitatively the same as previous runs. The same changes to hmF2, NmF2, and ThF2 are observed with the June solstices when compared to December. Though the depression in ThF2 during the day remains clear, as the latitudinal width of the COSMIC data increases, the increase in ThF2 just before dawn is not as prevalent. The dominant modes for ThF2 still show the same behaviors as shown here when using data within $\pm 15°$ GLAT, including the predawn increase in ThF2. Both the RMS and reconstruction error when using 9 day medians and measurements between $\pm 25°$ MLAT are less than 5 m/s for meridional ion drifts. The reduction in the meridional ion drift estimations is a result of the increased COSMIC coverage as CINDI measurements remained restricted to $\pm 5°$ MLAT.

[53] The normalization of the input data sets by the maximum deviation from the mean employed allows for the possibility of noise in the input data to significantly alter the normalization and impact the specific covariances calculated by DINEOFs. While care was taken in producing a clean input data set, to ensure the conclusions presented are robust, the more common normalization by the standard deviation was also utilized. Processing input data by removing the mean and normalizing by the standard deviation for each different measurement type or by using the mean and standard deviation of each input array element in time produced no significant changes in the reconstruction characteristics of $F10.7$, *Dst*, C/NOFS, or COSMIC data. Reconstruction of the seasonal sine and cosine inputs was degraded when normalizing by the standard deviation compared to using the maximum deviation. The cosine mode is still reproduced though with a larger variance around the input waveform. When normalizing by the maximum value, this equinoctial variation is described in a single mode while the use of the standard deviation for normalization spreads this variation across multiple DINEOF modes. For the solstice sine wave, only the most general characteristics are reproduced. The solstice waveform has a significant correlation with the $F10.7$ waveform while also having smaller normalized (by standard deviation) deviations from the mean. The choice of a standard deviation normalization makes changes in $F10.7$ more significant while the general correlation of $F10.7$ and solstice in time places both of these inputs in competition. Thus, we find that the fidelity in which particular variations in a given data set may be isolated is impacted by normalization choices but the overall characteristics of the reconstruction are not.

4.1. Future Work

[54] DINEOF reconstructions of the ionosphere could be improved by incorporating ion drift measurements from multiple platforms. Ion drifts measured by ground stations such as the Jicamarca Radar Observatory along with in situ satellite measurements from Defense Meteorological Satellite Program (DMSP) and C/NOFS could all be combined. Jicamarca Radar Observatory (JRO) observes a fixed location at all local times (given sufficient signal) while the polar orbit of DMSP confines measurements to all longitudes and a range of magnetic local times near sunrise and sunset. C/NOFS has an equatorial orbit and makes about 15 passes around the globe per day, with quality drift measurements restricted by ambient density levels. The different measurement tracks of each platform provide different perspectives upon the ionosphere and the additional data should provide for more accurate DINEOF reconstructions that also accounts for longitudinal variations.

[55] Ion drift data from each instrument could be combined into a single array covering longitude and local time and analyzed with DINEOFs. At locations with multiple measurements, a method of combining the measurements would need to be used. Alternatively, the measurements from each platform could be treated separately. Adding JRO and DMSP measurements to the DINEOF process can be accomplished by including the data as additional rows in data set $\mathbf{X}$. Since the individual platforms could have a relative bias between the instruments, by separating out each instrument, the DINEOF process determines the relative associations between the instruments when performing the reconstruction. However, in this configuration, there is a drift reconstruction for each instrument yielding multiple drift predictions wherever instrument coverage overlaps.

[56] CINDI and COSMIC data may also be combined to produce a specification of parallel or field-aligned ion drifts. The movement of plasma along the field line has an impact on the relative levels of NmF2 and hmF2 at latitudes away from the equator in the Northern and Southern Hemispheres [*Burrell et al.*, 2011]. The physical relationship between the COSMIC measurements away from the equator as well as the in situ field-aligned drifts and meridional drifts [*Burrell et al.*, 2012] may be exploited to produce a similar reconstruction for these quantities. Given the relationship to the meridional drifts, it may be possible to incorporate this additional information with the model presented here.

[57] For the equatorial ionosphere, physical boundary conditions may also be incorporated into the DINEOF process to improve reconstructions. The mean meridional drifts over all local times and longitudes are required to be zero to maintain a curl-free electric field. In principle, this requirement could be determined from the data alone, provided sufficient data coverage. The requirement of zero mean meridional drifts can be explicitly incorporated into the DINEOF iterative process by subtracting the mean of all meridional drifts for each time slice from the DINEOF estimated drifts at missing data locations each iteration.

[58] The curl-free condition of the electric field is also satisfied by the tidal components, diurnal, semi-diurnal, etc. that comprise the net electric field and ion drift around the ionosphere. Thus, in addition to requiring a zero meridional drift for the net reconstructions, a zero meridional drift may also be useful as a constraint on the individual DINEOF basis functions.

[59] The averages presented to DINEOFs have periodic boundary conditions across $0, 24$ local time as well as $0°, 360°$ longitude. As no a priori information about the data has been supplied to the DINEOF process, the continuity of the ionosphere across these boundaries is not required. It may be possible to encourage continuity across periodic boundary conditions when data coverage is sparse. The data set $\mathbf{X}$ could be expanded to include measurements at an imposed periodic boundary where all measurements at the boundary are treated as missing. As DINEOFs iterate to estimate these missing values, the mean of the points on either side of the boundary may be substituted for the DINEOF estimated value. With each iteration, continuity is assumed across the boundary and this assumption influences the DINEOF determined basis functions on the next iteration. The boundary condition will only affect the reconstructed drifts and basis functions on either side of the boundary if there is a significant covariance between these locations. As the boundary condition is expressed here as a mean of the surrounding points, a significant covariance is expected.

[60] These basic properties of the ionosphere may be useful as the objective measures needed for EOF rotations [*Hannachi et al.*, 2007]. Both orthogonal and nonorthogonal rotations are available that can determine a combination of modes that best satisfy the requirements. Due to the difficulties in establishing an offset correction for satellite measurements of drifts with no residual, a linear combination of basis functions that minimize the absolute mean of the drift modes may be a more useful rotation condition than a zero mean. Though the rotated basis functions are still not guaranteed to isolate physical sources, basis functions that best explain a long data set and also satisfy geophysical constraints upon the ionosphere could reveal additional physical information about the ionosphere.

[61] The upcoming COSMIC II mission offers the possibility of a constellation of satellites performing both in situ and RO measurements of the ionosphere. With the additional data, we hope to form reconstructions of NmF2 and hmF2 in longitude, latitude, and local time that can be used with in situ measurements of ion density to estimate scintillation measured on the ground [*Basu et al.*, 1988; *Wernik et al.*, 2007; *Stoneback et al.*, 2013]. In situ measurements of ion density can characterize plasma irregularities around the satellite accurately; however, the largest impact to a radio signal occurs at the largest absolute density change in the ionosphere. Since a satellite will generally not be at the density maximum, normalized in situ observations of irregularities may be scaled to the peak ion density assuming that $\Delta N/N$ remains constant along a flux tube if the maximum ionospheric density is known. *Wernik et al.* [2007] use the International Reference Ionosphere (IRI) to scale observed irregularities to the peak in ion density, though IRI has only limited capability in reproducing the day-to-day variability of the ionosphere. With complete maps of NmF2 and hmF2 from DINEOFs on a daily basis, in situ density measurements may be converted to a more accurate scintillation index. DINEOFs could be applied again to the in situ scintillation and combined with RO estimates of scintillation, as well as ground-based measurements, to produce a modal analysis of scintillation and provide an estimate for any gaps in the data set.

[62] The DINEOF process may also be useful in predicting space weather. Instead of determining basis functions describing the ionosphere over a single day, basis functions may be determined that describe the evolution of the ionosphere over several days [*Alvera-Azcárate et al.*, 2007]. If the DINEOF basis functions span p days, supplying data for q days where $q < p$ will provide a prediction for the remaining days. This prediction is generated using basis functions that best describe the data set. Thus, a long data set that includes the most significant drivers of a system may be effective at predicting the future state of the system. Given that the basis functions derived by DINEOFs best describe the data at hand, a system with sufficient high-quality data could be capable of accurate predictions. While the DINEOF model presented here was not able to relate *Dst* variations to changes in the ionosphere, one of the DINEOF models did produce an ionospheric response to a SSW consistent with previous measurements. Thus, we believe that as a general technique, DINEOFs could be useful for predicting short-term variations in the ionosphere given sufficient measurements even if the presented work is not always capable of this achievement.

[63] The future state of the ionosphere significantly depends upon the space weather inputs to the system. A full prediction of the ionosphere thus also requires a prediction of these inputs. Without a specification of the future inputs, DINEOF predictions would be based upon the presumption that existing trends in solar inputs would continue. This will obviously lead to errors when the actual solar inputs diverge from predictions. However, as the solar inputs change, these changes are reflected in the state of the ionosphere that will translate to changes in the DINEOF reconstructions.

5. Conclusion

[64] A combination of CINDI and COSMIC data produced a set of modes that span meridional ion drift, NmF2, hmF2, ThF2, $F10.7$, *Dst*, as well as time of year. Reconstructions with DINEOFs increased in accuracy with the inclusion of these different measurements relative to using CINDI meridional drifts alone. The different parameters are coupled via the covariance between parameters and measurement locations in the data set. The most significant mode identifies a base, generally static ionosphere. This mode follows general expectations for meridional ion

drift though drifts are weakly downward in the afternoon. Higher order modes account for seasonal and *F*10.7 changes though *Dst* changes are not well represented. An improved DINEOF specification of the ionosphere during geomagnetic disturbances might be achieved by including additional space weather parameters or data sets.

[65] During the June solstices, the ionosphere departs from conditions that dominate the other seasons, reflected in both COSMIC measurements of NmF2, hmF2, and ThF2 as well as CINDI measurements of ion drift, validating measurements from both platforms. The annual anomaly in ionospheric density has been reported previously [*Berkner and Wells*, 1938; *Rishbeth*, 1998, 2004; *Zeng et al.*, 2008; *Burns et al.*, 2012] and reflects an increased NmF2 in December when compared to June. The change in the equatorial ionosphere during the June solstices is consistent with the change in meridional ion drift reported here, though the cause of the drift perturbation is not known. Changing the altitude of the ionosphere near the equator with meridional ion drifts leads to field-aligned plasma motions called the "fountain effect" which produces the equitorial ionization anomaly crests. Thus, the reported change in meridional ion drift will also impact ionospheric densities at latitudes away from the magnetic equator. Though *F*10.7 cm flux has relative minima during the June solstice seasons, the June solstice of 2010 has a higher *F*10.7 flux than January 2009; thus, the seasonal changes to the ionosphere measured by COSMIC are not solely due to changes in solar output.

[66] The DINEOF process has a number of advantages for studies of the ionosphere. Satellite data are often incomplete and DINEOFs can provide a best guess at the value of missing data locations. DINEOFs can incorporate multiple types of measurements of the ionosphere, whether from the ground or satellite, and can accommodate the different spatial characteristics of each instrument. As shown, with these properties, DINEOFs can be used to integrate a number of different ionospheric measurements, provided the measurements have an underlying physical relationship, to produce a single data-based model of the ionosphere.

[67] **Acknowledgments.** Work is supported at UT Dallas by NASA grant NNX10AT029.

[68] Robert Lysak thanks Hee-Jeong Kim and two anonymous reviewers for their assistance in evaluating this paper.

References

A, E., D. Zhang, A. J. Ridley, Z. Xiao, and Y. Hao (2012), A global model: Empirical orthogonal function analysis of total electron content 1999–2009 data, *J. Geophys. Res.*, *117*, A03328, doi:10.1029/2011JA017238.

Alvera-Azcárate, A., A. Barth, and M. Rixen (2005), Reconstruction of incomplete oceanographic data sets using empirical orthogonal functions: Application to the Adriatic Sea surface temperature, *Ocean Model.*, *9*, 325–346

Alvera-Azcárate, A., A. Barth, J. M. Beckers, and R. H. Weisberg (2007), Multivariate reconstruction of missing data in sea surface temperature, chlorophyll, and wind satellite fields, *J. Geophys. Res.*, *112*, C03008, doi:10.1029/2006JC003660.

Alvera-Azcárate, A., A. Barth, D. Sirjacobs, and J. M. Beckers (2009), Enhancing temporal correlations in EOF expansions for the reconstruction of missing data using DINEOF, *Ocean Sci.*, *5*(4), 475–485.

Basu, S., S. Basu, E. J. Weber, and W. R. Coley (1988), Case study of polar cap scintillation modeling using DE 2 irregularity measurements at 800 km, *Radio Sci.*, *23*(4), 545–553.

Beckers, J. M., and M. Rixen (2003), EOF calculations and data filling from incomplete oceanographic datasets, *J. Atmos. Oceanic Technol.*, *20*, 1839–1856.

Beckers, J. M., A. Barth, and A. Alvera-Azcárate (2006), DINEOF reconstruction of clouded images including error maps. Application to the Sea-Surface Temperature around Corsican Island, *Ocean Sci.*, *2*(2), 183–199.

Berkner, L. V., and H. W. Wells (1938), Non-seasonal change of F 2-region ion-density, *J. Geophys. Res.*, *43*(1), 15.

Burkard, O. (1951), Die halbjährige Periode derF 2-Schicht-Ionisation, *Institut für Meteorologie und Geophysik*, *4*(1), 391–402.

Burns, A. G., S. C. Solomon, W. Wang, L. Qian, Y. Zhang, and L. J. Paxton (2012), Daytime climatology of ionospheric NmF2 and hmF2 from COSMIC data, *J. Geophys. Res.*, *117*, A09315, doi:10.1029/2012JA017529.

Burrell, A. G., R. A. Heelis, and R. Stoneback (2011), Latitude and local time variations of topside magnetic field-aligned ion drifts at solar minimum, *J. Geophys. Res.*, *116*, A11312, doi:10.1029/2011JA016715.

Burrell, A. G., R. A. Heelis, and R. Stoneback (2012), Equatorial longitude and local time variations of topside magnetic field-aligned ion drifts at solar minimum, *J. Geophys. Res.*, *117*, A04304, doi:10.1029/2011JA017264.

Chau, J. L., B. G. Fejer, and L. P. Goncharenko (2009), Quiet variability of equatorial E x B drifts during a sudden stratospheric warming event, *Geophys. Res. Lett.*, *36*(5), L05101, doi:10.1029/2008GL036785.

Cheng, C.-Z. F., Y.-H. Kuo, R. A. Anthes, and L. Wu (2006), Satellite constellation monitors global and space weather, *Eos*, *87*(1), 166–166.

Fejer, B. G. (2011), Low latitude ionospheric electrodynamics, *Space Sci. Rev.*, *158*, 145–166.

Fejer, B. G., S. A. Gonzalez, E. R. de Paula, and R. F. Woodman (1991), Average vertical and zonal F region plasma drifts over Jicamarca, *J. Geophys. Res.*, *96*(A8), 13,901–13,906.

Fuller Rowell, T., F. Wu, R. Akmaev, T. W. Fang, and E. Araujo-Pradere (2010), A whole atmosphere model simulation of the impact of a sudden stratospheric warming on thermosphere dynamics and electrodynamics, *J. Geophys. Res.*, *115*, A00G08, doi:10.1029/2010JA015524.

Golovkov, V. P., T. I. Zvereva, and T. A. Chernova (2007), Space-time modeling of the main magnetic field by combined methods of spherical harmonic analysis and natural orthogonal components, *Geomag. Aeron.*, *47*, 256–262.

Goncharenko, L. P., J. L. Chau, and H.-L. Liu (2010), Unexpected connections between the stratosphere and ionosphere, *Geophys. Res. Lett.*, *37*, L10101, doi:10.1029/2010GL043125.

Habarulema, J. B., L.-A. McKinnell, and B. D. L. Opperman (2011), Regional GPS TEC modeling; Attempted spatial and temporal extrapolation of TEC using neural networks, *J. Geophys. Res.*, *116*, A04314, doi:10.1029/2010JA016269.

Hannachi, A., I. T. Jolliffe, and D. B. Stephenson (2007), Empirical orthogonal functions and related techniques in atmospheric science: A review, *Int. J. Climatol.*, *27*(9), 1119–1152.

Heelis, R. A., and W. Hanson (1998), Measurements of thermal ion drift velocity and temperature using planar sensors, in *Measurement Techniques in Space Plasmas: Particles, Geophys. Monogr. Ser.,* vol. 102, edited by F. Pfaff, E. Borovsky, and T. Young, pp. 61–71, AGU, Washington, D. C.

Heelis, R. A., et al. (2009), Behavior of the O+/H+ transition height during the extreme solar minimum of 2008, *Geophys. Res. Lett.*, *36*, L00C03, doi:10.1029/2009GL038652.

Huang, C., S. H. Delay, P. A. Roddy, E. K. Sutton, and R. Stoneback (2012), Longitudinal structures in the equatorial ionosphere during deep solar minimum, *J. Atmos. Sol. Terr. Phys.*, *90-91*, 156–163.

Hwang, C., T. P. Tseng, T. J. Lin, D. Švehla, and U. Hugentobler (2010), Quality assessment of FORMOSAT-3/COSMIC and GRACE GPS observables: Analysis of multipath, ionospheric delay and phase residual in orbit determination, *GPS solutions*, *14*, 121–131.

Kelley, M. C. (2009), *The Earth's Ionosphere: Plasma Physics and Electrodynamics,* 2nd ed., Elsevier, Boston, Mass.

Kil, H., S.-J. Oh, L. J. Paxton, and T.-W. Fang (2009), High-resolution vertical E x B drift model derived from ROCSAT-1 data, *J. Geophys. Res.*, *114*, A10314, doi:10.1029/2009JA014324.

Kim, H.-J., L. R. Lyons, J. M. Ruohoniemi, N. A. Frissell, and J. B. Baker (2012), Principal component analysis of polar cap convection, *Geophys. Res. Lett.*, *39*, L11105, doi:10.1029/2012GL052083.

Kuttippurath, J., and G. Nikulin (2012), The sudden stratospheric warming of the Arctic winter 2009/2010: Comparison to other recent warm winters, *Atmos. Chem. Phys. Discuss.*, *12*(3), 7243–7271.

Lei, J., et al. (2007a), Comparison of COSMIC ionospheric measurements with ground-based observations and model predictions: Preliminary results, *J. Geophys. Res.*, *112*, A07308, doi:10.1029/2006JA012240.

Lin, C. H., C. C. Hsiao, J. Y. Liu, and C. H. Liu (2007b), Longitudinal structure of the equatorial ionosphere: Time evolution of the four-peaked EIA structure, *J. Geophys. Res.*, *112*, A12305, doi:10.1029/2007JA012455.

Liu, L., B. Zhao, W. Wan, B. Ning, M.-L. Zhang, and M. He (2009), Seasonal variations of the ionospheric electron densities retrieved from constellation observing system for meteorology, ionosphere, and climate mission radio occultation measurements, *J. Geophys. Res.*, *114*, A02302, doi:10.1029/2008JA013819.

Pacheco, E. E., R. A. Heelis, and S. Y. Su (2010), Quiet time meridional (vertical) ion drifts at low and middle latitudes observed by ROCSAT-1, *J. Geophys. Res.*, *115*, A09308, doi:10.1029/2009JA015108.

Patra, A. K., P. P. Chaitanya, N. Mizutani, Y. Otsuka, T. Yokoyama, and M. Yamamoto (2012), A comparative study of equatorial daytime vertical E x B drift in the Indian and Indonesian sectors based on 150 km echoes, *J. Geophys. Res.*, *117*, A11312, doi:10.1029/2012JA018053.

Pfaff, R., D. Rowland, and H. Freudenreich (2010), Observations of DC electric fields in the low-latitude ionosphere and their variations with local time, longitude, and plasma density during extreme solar minimum, *J. Geophys. Res.*, *115*, A12324, doi:10.1029/2010JA016023.

Preisendorfer, R. W. (1988), *Principal Component Analysis in Meteorology and Oceanography*, Elsevier, New York.

Rishbeth, H. (1998), How the thermospheric circulation affects the ionospheric F2-layer, *J. Atmos. Sol. Terr. Phys.*, *60*(1), 1385–1402.

Rishbeth, H. (2004), Questions of the equatorial F2-layer and thermosphere, *J. Atmos. Sol. Terr. Phys.*, *66*(1), 1669–1674.

Schreiner, W. S., S. V. Sokolovskiy, C. Rocken, and D. C. Hunt (2012), Analysis and validation of GPS/MET radio occultation data in the ionosphere, *Radio Sci.*, *34*(4), 949–966, doi:10.1029/1999RS900034.

Stoneback, R., R. A. Heelis, A. G. Burrell, W. R. Coley, B. G. Fejer, and E. Pacheco (2011), Observations of quiet time vertical ion drift in the equatorial ionosphere during the solar minimum period of 2009, *J. Geophys. Res.*, *116*, A12327, doi:10.1029/2011JA016712.

Stoneback, R., R. L. Davidson, and R. A. Heelis (2012), Ion drift meter calibration and photoemission correction for the C/NOFS satellite, *J. Geophys. Res.*, *117*, A08323, doi:10.1029/2012JA017636.

Stoneback, R. A., R. A. Heelis, R. G. Caton, Y.-J. Su, and K. M. Groves (2013), In situ irregularity identification and scintillation estimation using wavelets and CINDI on C/NOFS, *Radio Sci.*, *48*, 388–395, doi:10.1002/rds.20050.

Sun, W., W. Y. Xu, and S. I. Akasofu (1998), Mathematical separation of directly driven and unloading components in the ionospheric equivalent currents during substorms, *J. Geophys. Res.*, *103*(A6), 11,695–11,700.

Toumazou, V., and J. Cretaux (2001), Using a Lanczos eigensolver in the computation of empirical orthogonal functions, *Mon. Weather Rev.*, *129* (5), 1243–1250.

Wernik, A., L. Alfonsi, and M. Materassi (2007), Scintillation modeling using in situ data, *Radio Sci.*, *42*, RS1002, doi:10.1029/2006RS003512.

Yue, X., W. S. Schreiner, J. Lei, S. V. Sokolovskiy, C. Rocken, D. C. Hunt, and Y.-H. Kuo (2010), Error analysis of Abel retrieved electron density profiles from radio occultation measurements, *Ann. Geophys.*, *28*(1), 217–222.

Zeng, Z., A. Burns, W. Wang, and J. Lei (2008), Ionospheric annual asymmetry observed by the COSMIC radio occultation measurements and simulated by the TIEGCM, *J. Geophys. Res.*, *113*, A07305, doi:10.1029/2007JA012897.